ELSEVIER

Catalysis Today 64 (2001) 321–332

CATALYSIS TODAY

www.elsevier.com/locate/cattod

Liquid back-mixing in packed-bubble column reactors: a state-of-the-art correlation

Lamia Belfares [a], Miryan Cassanello [b], Bernard P.A. Grandjean [a], Faïçal Larachi [a,*]

[a] Department of Chemical Engineering and CERPIC, Université Laval, Ste-Foy, Québec, Canada G1K 7P4

[b] PINMATE, Departmento de Industrias, Facultad de Ciencias Exactas y Naturales, Universidad de Buenos Aires, Ciudad Universitaria, 1428 Buenos Aires, Argentina

Abstract

The extent of liquid back-mixing in gas–liquid concurrent upflow packed-bubble column reactors is quantified in terms of an axial dispersion coefficient or its corresponding dimensionless Péclet number. Effects of reactor operating conditions on the axial dispersion coefficient are not properly accounted for by the available literature correlations, wherein most often the Péclet number is expressed solely in terms of the gas and liquid Reynolds numbers or superficial velocities. Based on the broadest experimental databank (1322 measurements, 11 liquids, four gases, 28 packing materials, 14 columns diameters, Newtonian, non-Newtonian, aqueous, organic, coalescing and non-coalescing liquids, high pressure, bubble and pulsing flow regime conditions), a state-of-the-art liquid axial dispersion coefficient correlation is obtained by combining neural network modeling and dimensional analysis. Thorough qualitative and quantitative analyses of the constructed databank demonstrate the robustness of the proposed correlation to restore the variety of trend variations of liquid Péclet numbers reported in the literature.

Keywords: Gas–liquid upflow; Packed-bubble column; Liquid back-mixing; Neural network

1. Introduction

Catalytic three-phase fixed-bed reactors involving concurrent gas–liquid upflow, or packed-bubble columns (PBCs), are an offshoot of the conventional trickle-bed reactors (concurrent downflow configuration). The higher holdup and better cross-sectional distribution of the liquid phase in PBCs make them superior to trickle beds with respect to heat withdrawal and wetting efficiency [1,2]. Due to the prevailing full pellet-scale wetting conditions, liquid-limited reactions are more propitiously run in PBCs, wherein higher conversions can be attained. Moreover, pilot and laboratory-scale PBCs are massively used in the petroleum industries for the assessment of alternative feed stocks or for the testing of catalyst efficiency.

One major setback in PBC hydrodynamics is the significance of liquid back-mixing which can be detrimental to the reactor performance [3,4]. Especially critical at high conversions in small-scale PBCs, the entanglement between liquid back-mixing and intrinsic kinetics can be the cause of negative repercussions in scale-up and reactor design [5,6].

Among the plethora of liquid back-mixing quantifiers encountered in the literature, the axial dispersion coefficient (D_{ax}), or its dimensionless pendant, i.e., the particulate-scale Péclet number (*Pe*), are the ones most frequently used. A scrutinizing examination of literature information regarding D_{ax} (or *Pe*) reveals that the rare correlations available for PBCs have not

* Corresponding author. Tel.: +1-418-656-3566; fax: +1-418-656-5993.
E-mail address: flarachi@gch.ulaval.ca (F. Larachi).

PII: S0920-5861(00)00535-6

Nomenclature

a	external surface area per unit volume of particle (m^2/m^3)
a_s	specific surface area of the porous medium column assemblage, $a_s = 6(1-\varepsilon)/\phi d_{eq} + 4/d_c$ (m^2/m^3)
AARE	average absolute relative error, $\mathrm{AARE} = (1/N)\sum_{i=1}^{N} \lvert (y_{mes}(i) - y_{pred}(i))/y_{mes}(i)\rvert$
Ca_L	liquid capillary number, $Ca_L = u_{LS}\mu_L/\sigma_L$
d_c	column diameter (m)
d_h	Krischer and Kast hydraulic diameter, $d_h = d_{eq}\sqrt[3]{16\varepsilon^3/9\pi(1-\varepsilon)^2}$
d_{eq}	grain equivalent diameter, diameter of sphere having same volume as the grain (m)
d_s	grain equivalent diameter, diameter of sphere having same surface as the grain (m)
D_L	tracer diffusivity in liquid-phase (m^2/s)
$E\ddot{o}_m$	modified Eötvös number, $E\ddot{o}_m = \rho_L g d_{eq}^2 \phi^2 \varepsilon^2/\sigma_L(1-\varepsilon)^2$
Fr_G	gas Froude number, $Fr_L = u_{GS}^2/gd_{eq}$
g	gravitational acceleration (m/s^2)
H	hidden-layer vector
J	number of nodes in hidden layer
N	number of data
P	pressure (MPa)
Pe_{d0}	Péclet number based on the interstitial liquid velocity, Pe_d/ε_L
Pe_d	Péclet number based on the superificial liquid velocity, $Pe_d = u_{LS}d_{eq}/D_{ax}$
R	cross-correlation coefficient between measured and predicted values, $R = \sum_{i=1}^{N}(y_{mes}(i) - y_{mes,mean})(y_{pred}(i) - y_{pred,mean})/\left(\sum_{i=1}^{N}(y_{mes}(i) - y_{mes,mean})^2\right)^{1/2}\left(\sum_{i=1}^{N}(y_{pred}(i) - y_{pred,mean})^2\right)^{1/2}$
Re_α	α-phase Reynolds number, $Re_\alpha = u_{\alpha S}\rho_\alpha d_{eq}/\mu_\alpha$
S	network output
S_b	bed correction function, $S_b = a_s d_h/(1-\varepsilon)$
Sc_L	liquid-phase Schmidt number, $Sc_L = \mu_L/D_L\rho_L$
St_L	liquid Stokes number, $St_L = u_{LS}\mu_L/g\rho_L d_{eq}^2$
U_i	normalized input variables
u_{GS}	superficial gas velocity (m/s)
u_{LS}	superficial liquid velocity (m/s)

Greek letters

α	subscript meaning gas (G) or liquid (L)
ε	bed void fraction
ε_L	liquid holdup
μ_α	α-phase dynamic viscosity (kg/m s)
ξ	two phase flow dissipation power rate, $\xi = (\Delta P/Z)(u_{LS} + u_{GS})/\varepsilon + g(\rho_L u_{LS} + \rho_G u_{GS})/\varepsilon$ (Pa/s)
ρ_α	α-phase density (kg/m^3)
σ	standard deviation, $\sigma = \left(\sum_{i=1}^{N}[\lvert(y_{pred}(i) - y_{mes}(i))/y_{mes}(i)\rvert - \mathrm{AARE}]^2/(N-1)\right)^{1/2}$
σ_L	surface tension (N/m)
ϕ	sphericity factor
ω	weights

Subscripts

pred	predicted
mes	measured
G	gas
L	liquid

always succeeded at providing reliable estimations of these parameters. Two factors are responsible for this state of affairs: (i) the apparent incoherence of literature which reports contradictory conclusions regarding the trend variations of D_{ax} (or *Pe*) as a function of operating conditions; (ii) the narrowness of ranges in all the developed correlations renders them vulnerable and of limited value when venturing outside the validity domain of experimental conditions.

In an effort to develop a more general correlation of the liquid Péclet number that reconciles the various trend patterns of liquid back-mixing in PBCs, use is made in this work of perceptron neural network modeling, dimensional analysis and the largest historic flow

Table 1
Summary of axial dispersion coefficient studies in packed-bubble column reactors

Reference	System	Column	Packing	Model used and proposed correlation
Bill [12]	Air/water	30 mm ID	3 mm × 10 mm porous extrudates ($\varepsilon = 0.53$)	PD model
Weber [13]	Air/water	50 mm ID	2 and 5 mm spheres ($\varepsilon = 0.32$)	PD model, (a) $Pe_{d0} = 0.012[Re_L(u_L/u_G)Sc_L]^{0.48}$, $u_{LS} = 0.057$–5.1 mm/s, $u_{GS} = 2.12$–28 mm/s[a]
	Air/water + sugar		3.8 mm × 10 mm cylinders ($\varepsilon = 0.42$)	PD model, (b) $Pe_{d0} = 0.024\left[Re_L\left(\frac{u_L}{u_G}\right)Sc_L\right]^{0.46}$, $u_{LS} = 0.057$–5.1 mm/s, $u_{GS} = 2.12$–28 mm/s
	Air/water + ethanol		6.2 mm × 6.2 mm Raschig rings ($\varepsilon = 0.71$)	PD model, (c) $Pe_{d0} = 0.017\left[Re_L\left(\frac{u_L}{u_G}\right)Sc_L\right]^{0.43}$, $u_{LS} = 0.057$–5.1 mm/s, $u_{GS} = 2.12$–28 mm/s
Heilmann and Hofmann [14]	Air/water	150 mm ID	10 mm × 12 mm Raschig rings ($\varepsilon = 0.4$)	PD model, $Pe_{d0} = \frac{\varepsilon_L}{470}\left[\frac{Re_L/\varepsilon_L}{\varepsilon_G d_p^{3.3}}\right]^{0.735}$, $u_{LS} = 5$–14.5 mm/s, $u_{GS} = 0.3$–40 mm/s
Bezdenezhnykh et al. [15]	Air/water Air/glycerin	18–80 mm ID	3 mm × 5 mm porous cylinders ($\varepsilon = 0.35$)	PD model, $Pe_{d0} = 0.11\left(\frac{Re_L}{\varepsilon}\right)^{0.45}\left(\frac{Re_G}{\varepsilon}\right)^{0.47}\left(\frac{d_p}{d_c}\right)^{-0.31}$, $11 \le Re_G \le 265$, $0.565 \le Re_L \le 21$
Stiegel and Shah [16]	Air/water	51 mm ID	3.1 mm × 3.1 mm extrudates ($\varepsilon = 0.35$)	PD model, $Pe_{d0} = 0.128\,Re_G^{0.245}\,Re_L^{-0.16}(\mathrm{ad_s})^{0.53}$, $u_{LS} = 2.5$–33 mm/s, $u_{GS} = 20$–110 mm/s
Stiegel and Shah [17]	Air/water	Rectangular 168 mm × 20.6 mm	2.8 mm × 5.6 mm extrudates ($\varepsilon = 0.36$)	PD model, $Pe_{d0} = 0.0775\,Re_G^{0.31}\,Re_L^{-0.097}$, $u_{LS} = 5.4$–36 mm/s, $u_{GS} = 60$–750 mm/s
Achwal and Stepanek [18]	Air/water	51 mm ID	6 mm × 6 mm ceramic cylinders ($\varepsilon = 0.4$)	PD model, $Pe_d = 6.52u_{LS}^{0.416}10^{-0.384u_{GS}}$, $u_{LS} = 18$–85 mm/s, $u_{GS} = 0.5$–380 mm/s
Skomorokov et al. [24]	Air/water	30 mm ID	3 mm × 3 mm glass cylinders ($\varepsilon = 0.37$)	PDE model
Yang [27]	Air/water	25 mm ID	2.2 mm porous spheres ($\varepsilon = 0.31$)	PD model
van Gelder and Westerterp [19]	Hydrogen/toluene	65 mm ID	3.8 mm × 4.82 mm glass cylinders ($\varepsilon = 0.37$)	PD model, $Pe_{d0} = 0.12u_{LS}^{0.310}u_{GS}^{-0.177}$, $u_{LS} = 0.05$–0.15 mm/s, $u_{GS} = 0.5$–14 mm/s
Thanos et al. [20]	Nitrogen/toluene	20 mm ID	1.2–2 mm × 2.7–6.8 mm extrudates ($\varepsilon = 0.365$–0.453)	PD model
Illiuta et al. [25]	Air/water	51 mm ID	3 mm glass spheres ($\varepsilon = 0.37$)	PDE model plus intraparticle diffusion in the case of porous grains

Table 1 (*Continued*)

Reference	System	Column	Packing	Model used and proposed correlation
	Air/water + CMC		3.3 mm porous spheres ($\varepsilon = 0.356$)	
Cassanello et al. [21,22]	Air/water	70 mm ID	5 and 16.7 mm glass spheres ($\varepsilon = 0.4, 0.47$)	PD model,
	Air/Water + Sugar			$Pe_{\mathrm{d}} = 0.05\,Re_{\mathrm{L}}^{0.53}\,Re_{\mathrm{G}}^{0.134}$,
				$Pe_{\mathrm{d}} = 0.026(Re_{\mathrm{L}}\xi)^{0.302}$ (for bubble flow regime),
				$u_{\mathrm{LS}} = 2.7\text{–}39\,\mathrm{mm/s}$, $u_{\mathrm{GS}} = 3.5\text{–}45\,\mathrm{mm/s}$
Haga et al. [31]	Air/water	41 mm ID	1 mm glass spheres ($\varepsilon = 0.373$)	PD model
Thanos et al. [32]	Nitrogen/toluene	25 mm ID	1.2 mm × 2.5 mm extrudates ($\varepsilon = 0.375$)	PD model
Thanos et al. [6]	Nitrogen/toluene	25 mm ID	1.2 mm × 2.5 mm extrudates ($\varepsilon = 0.375$)	PD model
	Hydrogen/toluene		1.5 mm × 5.3 mm extrudates ($\varepsilon = 0.403$)	
Stüber [34]	H_2/cyclododecatriene	26 mm ID	4 mm glass spheres ($\varepsilon = 0.4$)	PD model
Syaiful [35]	Air/water	95 mm ID	3 mm glass spheres ($\varepsilon = 0.4$)	PD model
	Air/glycerol + water			
	Air/NaOH			
	Air/xanthane			

[a] Correlation developed for 5 mm spheres.

databank of experimental axial dispersion coefficient measurements published in the open literature since 1955 (see Table 1 for a summary). The effectiveness of the proposed correlation is discussed through comparisons against the few rare literature *Pe*-correlations using systematic statistical tests across the constructed databank. The methodology leading to the neural network correlation is similar to the one already described in [7,8], and for brevity, will be skipped here.

2. Brief historic literature survey

The macro-mixing characteristics of the liquid phase in a gas–liquid–solid system is usually evaluated by residence time distribution (RTD) measurements. RTD information can be obtained by adding a pulse or a step of an inert tracer to the reactor influent and detecting its time dependent concentration in the effluent stream. The mixing parameters are then extracted by matching to the measured RTD and adequate RTD flow model. Several models, comprehensive reviews of which are provided in Refs. [9–11], are used to represent the flowing characteristics of the liquid phase. In the context of liquid back-mixing in PBCs, the most widely used RTD model is by far the "axial dispersion model" [12–22]. This model assumes a *P*iston-like advective flow on which axial *D*ispersion is superimposed (PD model). The PD model involves two fitting parameters, the total liquid holdup (or liquid space time) and the axial dispersion coefficient or the Péclet number. It has been argued in several papers [23–27] that the existing stagnant zones in PBCs, especially in those containing porous particles, are not well accounted for by the PD model. Therefore and accordingly, a variant of this model was used to capture this feature in the liquid flow. Under these circumstances, the "piston diffusion exchange (PDE)" model is used. The PDE model assumes axially dispersed flow of dynamic liquid (holdup) and an exchange with inactive (static + intraparticle) liquid (holdup) [24,27] or an exchange with static liquid (holdup) and intraparticle liquid [25,28,29]. Depending on the level of sophistication, two to five additional parameters are required to better fit this tail in the RTD response curves [23,28–30], i.e., the ratio between dynamic and total liquid holdups, the dynamic liquid–solid and static liquid–solid mass transfer coefficients, the dynamic-static liquid mass transfer coefficient, and the intraparticle effective diffusivity.

Several studies have thus far been carried out on the effect of the fluids velocities [12–14,16–18], column size [15,17,26,27], packing type [13,20], liquid properties [13,22,25], elevated pressure [6,19] on the liquid Péclet number. While there is a general agreement that the Péclet number increases with increasing superficial liquid velocity, considerable discrepancies regarding the effect of the other variables, as shown in Table 2, still persist. Furthermore, many expressions of the Péclet number have been in use due to the various definitions of the characteristic lengths and velocities. This contributed to the confusion especially when computing and comparing liquid axial dispersion coefficients from different sources (Table 1). To unify among all the studies that were gathered up in our databank for the ultimate derivation of a

Table 2
Reported effects of operating variables on liquid Péclet numbers in packed-bubble columns

Increase in	Effect on Péclet number	Remark
Liquid superficial velocity	Increase	
Gas superficial velocity	Decrease	$u_{GS} \leq 2\,mm/s$ Ref. [20]
	N/C[a]	$u_{GS} > 2\,mm/s$ Ref. [20]
Liquid viscosity	N/C	Refs. [15,21,22,25]
Surface tension	N/C	Ref. [13]
Pressure	No change	Refs. [6,19]
Particle diameter	Decrease	Ref. [13]
Column diameter	No change	Refs. [15,26]
Bed porosity	N/C	Refs. [13,20]

[a] No clear cut.

generalized correlation, the Péclet number is defined in the present study using the *superficial* liquid velocity and the equivalent grain diameter, d_{eq}, of the sphere of *equal volume* as the particle under consideration:

$$Pe_d = \frac{u_{LS} d_{eq}}{D_{ax}} \tag{1}$$

3. Development of the state-of-the-art liquid axial dispersion coefficient correlation

3.1. Databank

1322 axial dispersion coefficient measurements have been collected from 16 independent published studies embracing bubble flow and pulsing flow regimes published between 1955 and 1999 (11 liquids, pure and mixed, Newtonian and non-Newtonian, coalescing and non-coalescing, aqueous or organics; four gases up to 5.3 MPa; 28 porous and non-porous packing materials; cylindrical and rectangular columns of 14 diameters). For the sake of homogeneity, all the Péclet numbers collected were normalized into Pe_d as defined in Eq. (1) above. Table 1 lists the nature of the gas–liquid systems and dimensions of the columns and packings used in these studies. Accordingly, Table 3 lists the ranges of the fluid properties and operating conditions. These are depicted in Fig. 1a–f in the form of cumulative number fraction distributions highlighting the visited partitions and gaps left in the experimental studies. It is instructive to observe that these ranges are not uniformly covered with experiments. For example, 68% of liquid velocity values are less than 1 cm/s despite a 8.5 cm/s maximum value, and 70% of gas velocity values are less than 10 cm/s despite a maximum at 100 cm/s.

3.2. Dimensional analysis

The impact of fluid velocities, densities, viscosities, and surface tension, gravitational acceleration, grain size and shape, bed diameter and porosity on the Pe_d is analyzed through the whole databank. Based on considerations stated elsewhere [7,8], all these factors were combined into the forces and dimensionless groups believed to affect the liquid back-mixing. The forces to be considered are the liquid and gas inertial forces: $F_{IL} = \rho_L u_{LS}^2$, $F_{IG} = \rho_G u_{GS}^2$, liquid viscous force: $F_{VL} = \mu_L u_{LS}/d_{eq}$, liquid gravitational force: $F_{GL} = \rho_L g d_{eq}$, and capillary force: $F_C = \sigma_L/d_{eq}$. The last factor to be included is a structural function, S_b, which incorporates the sizes and shapes of the grains and the column [7]. For rectangular beds, the value of d_c in the expression of S_b is that of an equivalent cylindrical column having the same cross-sectional area.

The importance of these forces and the complexity of their dependence to D_{ax} can be roughly inspected using a cross-correlation analysis. As shown in Table 4, the liquid axial dispersion coefficient increases with increasing capillary, liquid inertia and viscous forces. However, as expected from the reported effects of some operating variables on Pe_d (Table 2), the low cross-correlation response with respect to gas inertial force, liquid gravitational force and structural function is ambiguous. Low cross-correlation coefficients do not necessarily mean marginal effects, but on the contrary pinpoints to complex *non-monotonic domain-sensitive* relationships between D_{ax} and the corresponding inputs.

3.3. Neural regression

Several sets of dimensionless groups, derived from the above analysis were selected and correlated using

Table 3
Intervals of operating conditions and input dimensionless groups

Fluid physical properties	Operating conditions	Limits of dimensionless groups
$790 \le \rho_L$ (Kg/m^3) ≤ 1200	$2.0 \times 10^{-5} \le u_{LS}$ (m/s) $\le 8.51 \times 10^{-2}$	$8.536 \times 10^{-7} \le Fr_G \le 29.685$
$5.5 \times 10^{-4} \le \mu_L$ (Pa s) $\le 26.6 \times 10^{-3}$	$1.57 \times 10^{-4} \le u_{GS}$ (m/s) ≤ 1.0	$61.047 \times 10^{-3} \le Re_L \le 648$
$29 \times 10^{-3} \le \sigma_L$ (N/m) $\le 73 \times 10^{-3}$	$0.1 \le P$ (MPa) ≤ 5.3	$2.01 \le S_b \le 29.2$
$8.0 \times 10^{-2} \le \rho_G$ (Kg/m^3) ≤ 4.3		$6.41 \times 10^{-8} \le St_L \le 1.9 \times 10^{-3}$
$8.8 \times 10^{-6} \le \mu_G$ (Pa s) $\le 1.82 \times 10^{-5}$		$3.793 \times 10^{-7} \le Ca_L \le 2.76 \times 10^{-3}$
		$4.822 \times 10^{-2} \le E\ddot{o}_m \le 29.822$
		$1.272 \times 10^{-3} \le Pe_d \le 29.966$

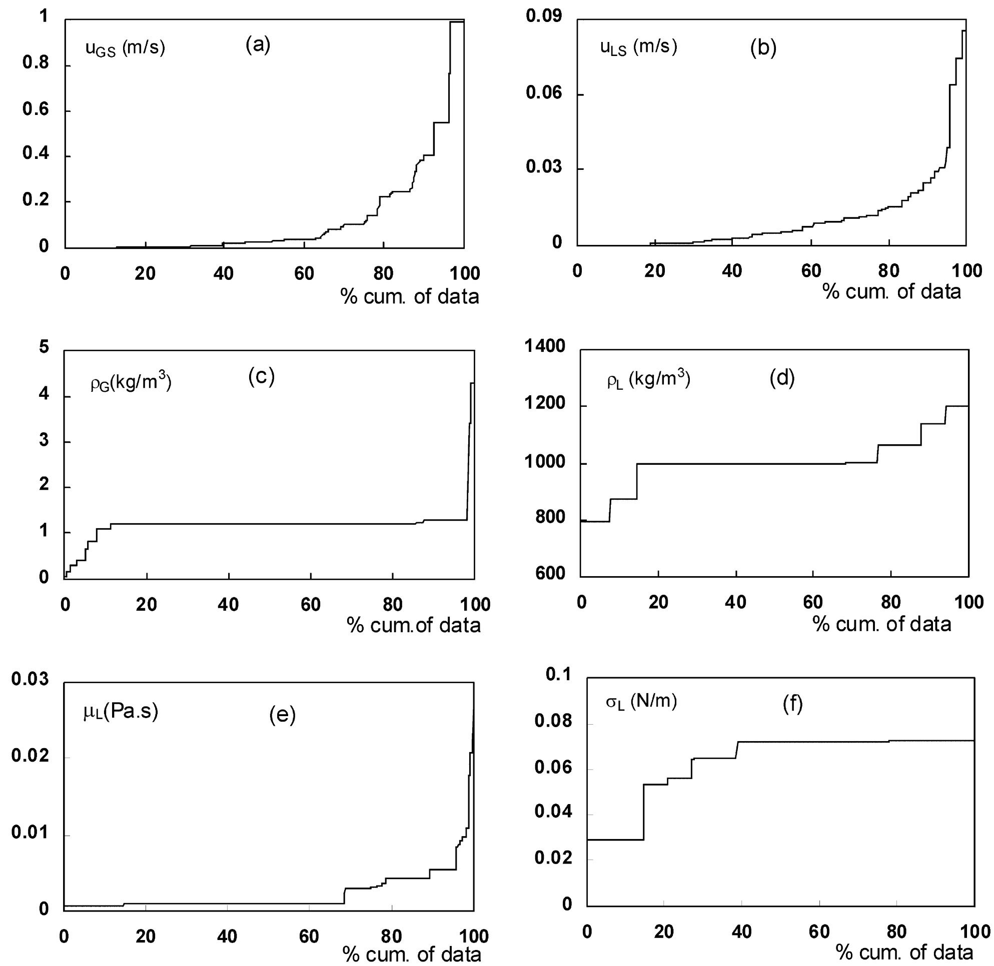

Fig. 1. Range variations of fluid velocities and properties in the databank.

Table 4
Cross-correlation coefficients between D_{ax} (resp. Pe_d) and forces (resp. resulting dimensionless groups)

Force	Cross-correlation to D_{ax} (%)	Dimensionless groups	Cross-correlation to Pe_d (%)
F_{IG}	−1.5	Fr_G	48
F_{GL}	−8	Re_L	19
F_C	18	S_b	−8
F_{IL}	19	St_L	−8
F_{VL}	21	Ca_L	11
S_b	−8	$E\ddot{o}_m$	25

artificial neural networks as a regression tool [7,8]. The optimal assortment of dimensionless groups intervening in the final Pe_d correlation is selected using a trial-and-error procedure which must fulfill the following criteria:

- the correlation must contain a minimum number of selected dimensionless numbers,
- the selected set must lead to the best match of output prediction, i.e., minimal absolute average relative error (AARE) and standard deviation, σ, and high cross-correlation coefficient, R, between predicted and measured Pe_d values on the learning and the test files altogether. For more details

on the procedure, the reader is referred to Refs. [7,8].

The set of dimensionless input variables of the neural network correlation is shown on Table 4 with the cross-correlation coefficients between each input and Pe_d. The three-layer neural network correlation chosen is described by

$$S = \frac{1}{1 + \exp\left[-\sum_{j=1}^{J+1} \omega_j H_j\right]} \tag{2}$$

$$H_j = \frac{1}{1 + \exp\left[-\sum_{i=1}^{I+1} \omega_{ij} U_i\right]} \tag{3}$$

In these equations, U and H define the input and hidden layer vectors, H_{J+1} and U_{I+1} are the bias constants set equal to 1, ω_{ij} and ω_j are the weighting factors, and J is the number of nodes in the hidden layer. The set of equations correlate the network output S,

$$S = \frac{\log(Pe_\mathrm{d}/1.272 \times 10^{-3})}{3.3676} \tag{4}$$

i.e. normalized Péclet particulate number, to a set of normalized input variables U_i,

$$U_1 = \frac{\log(Fr_\mathrm{G}/8.536 \times 10^{-7})}{7.5413},$$
$$U_2 = \frac{\log(Re_\mathrm{L}/61.047 \times 10^{-3})}{4.0258},$$
$$U_3 = \frac{S_\mathrm{b} - 2.01}{27.19}, \qquad U_4 = \frac{\log(St_\mathrm{L}/6.41 \times 10^{-8})}{4.3313},$$
$$U_5 = \frac{\log(Ca_\mathrm{L}/3.793 \times 10^{-7})}{3.862},$$
$$U_6 = \frac{\log(E\ddot{o}_\mathrm{m}/4.822 \times 10^{-3})}{2.7922}, \qquad U_7 = 1 \tag{5}$$

respectively, Fr_G, Re_L, S_b, St_L, Ca_L and $E\ddot{o}_\mathrm{m}$. The weighting factors for complete sets of the neural network equations (Eqs. (2)–(5)) are given in Table 5. In Fig. 2, the measured Pe_d are compared to those predicted by the neural correlation over the randomly sampled 926 learning data (filled symbol) and the 396 test data (empty symbol).

3.4. Comparison with literature correlations

The generalization capabilities of the literature correlations, listed in Table 1, were carried out based on AARE and σ, by testing them globally on the whole ranges of the databank as well as locally, i.e., on the correlation own authors' data. The results are summarized in Table 6.

In local tests (1st and 2nd entries in Table 6), the neural network correlation provides as good a prediction as on the proper author's measurements by the authors' own correlation. In the global tests, the performance of each literature correlation over the whole databank is given in the last column of Table 6. AARE by the neural network correlation is 4–155 times lower than any AARE given by the available Péclet number correlations.

A comparison between the neural network prediction of the Péclet numbers obtained with porous and non-porous particles is shown in Table 7 (first two entries). Interestingly, the prediction for the porous particles (Refs. [12,15,25,27]) is as good as for the non-porous ones (rest of the studies, Table 1), regardless of the RTD model used to fit Pe_d. Furthermore, no difference on the performance of the neural network correlation is detected whether Pe_d is inferred from the PDE or the PD models. This suggests that

Table 5
Weighting factors of the neural network correlation ($I = 6$, $J = 11$)

ω_{ij}	1	2	3	4	5	6	7	8	9	10	11	
1	−2.1172	−18.7758	−1.21994	1.32494	1.89511	3.84086	−0.519622	−0.011553	−1.66855	−1.1659	2.50028	
2	−4.2352	−88.3817	31.026	5.19268	−0.597487	−7.60127	6.21543	−5.05119	3.63475	11.7315	3.1395	
3	−2.90869	49.5161	−125.401	85.5363	−1.20334	−70.0686	−18.3445	−135.498	−2.76787	45.5414	−11.2716	
4	82.6329	−129.191	60.7947	107.804	−18.834	124.922	51.5102	47.148	−15.5833	−96.6862	−2.20575	
5	−24.2427	229.484	−38.9492	−102.649	16.0022	−111.077	−49.1595	−36.1592	8.63075	92.9329	−0.52716	
6	19.9201	−88.0117	1.6568	−6.54056	−10.7032	83.48	27.9552	−13.9368	6.42621	−0.559737	−2.25448	
7	−41.8797	10.9019	−43.8342	−18.6688	6.02487	−36.261	−16.9284	2.48399	0.988629	10.1696	−0.053743	
ω_j	1	2	3	4	5	6	7	8	9	10	11	12
	−0.63648	−0.42566	5.66213	−6.57653	−22.2734	3.4412	−7.9816	−5.3968	−5.5229	−8.15746	12.395	19.2604

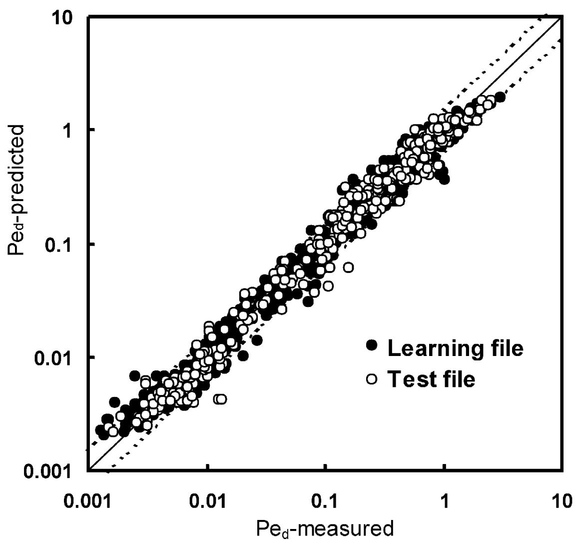

Fig. 2. Learning (●) and generalization (○) files parity plot. Predicted vs. measured Péclet particulate number.

the improvement in the prediction by the PDE model is not sufficient to overcome the uncontrollable experimental uncertainties on the determination of the axial dispersion. A further difficulty arises when Péclet number is estimated from the 4-parameter PDE model compared to the 2-parameter PD model.

Table 7
Performance of neural network correlation depending on RTD model and particle intra-porosity for Péclet prediction

Pe_d-data from	AARE (%)	σ (%)
Porous particles (400 data)	15	14
Non-porous particles (922 data)	20	18
PD model (porous and non-porous) (1150 data)	18	18
PDE (+intra-particle diffusion) model non-porous (porous) particles (172 data)	18	18

4. Effects of fluid and bed properties on the Péclet number

The neural network correlation can prove instructive to study how changes in fluid and bed properties can influence the liquid back-mixing in PBCs. A series of simulations (see Fig. 3 and Table 8 for its entry keys) is presented and discussed to check whether clear cuts can be drawn from varying the liquid and gas velocities, the liquid surface tension, the liquid viscosity, the particle diameter, the column diameter, and the bed porosity, and whether the simulated Pe_d values are consistent with experimental observations.

The gas density and viscosity are not included in the expressions of the input variables of the Pe_d

Table 6
Performance of neural network and available correlations to predict the Péclet number

References	Author's correlation on own data		Neural network correlation on author's own data		Author's correlation on whole databank (1322 data)	
	AARE (%)	σ (%)	AARE (%)	σ (%)	AARE (%)	σ (%)
Weber [13] — 25[a] (a)[b]	15	9	19	14	–	–
Weber [13] — 29 (b)	13	15	22	16	–	–
Weber [13] — 25 (c)	15	10	13	9	–	–
Bezdenezhnykh et al. [15] — 287	40	17	11	8	>500	>500
Stiegel and Shah [16] — 13	26	29	19	14	428	852
Stiegel and Shah [17] — 19	17	12	42	30	–	–
Achwal and Stepanek [18] — 93	23	14	18	12	>500	>500
Van Gelder and Westerterp [19] — 99	44	9	22	20	84	50
Cassanello et al. [21] — 112	45	19	20	20	>500	>500
Cassanello et al. [22] — 640	36	13	19	18	>500	>500
Kirillov et al. [33]	–	–	–	–	>500	>500
ANN, training file — 926	–	–	–	–	18	16.5
ANN, test file — 396	–	–	–	–	20	19
ANN correlation, whole data	–	–	–	–	19	17

[a] Number of data.
[b] See Table 1 for these references.

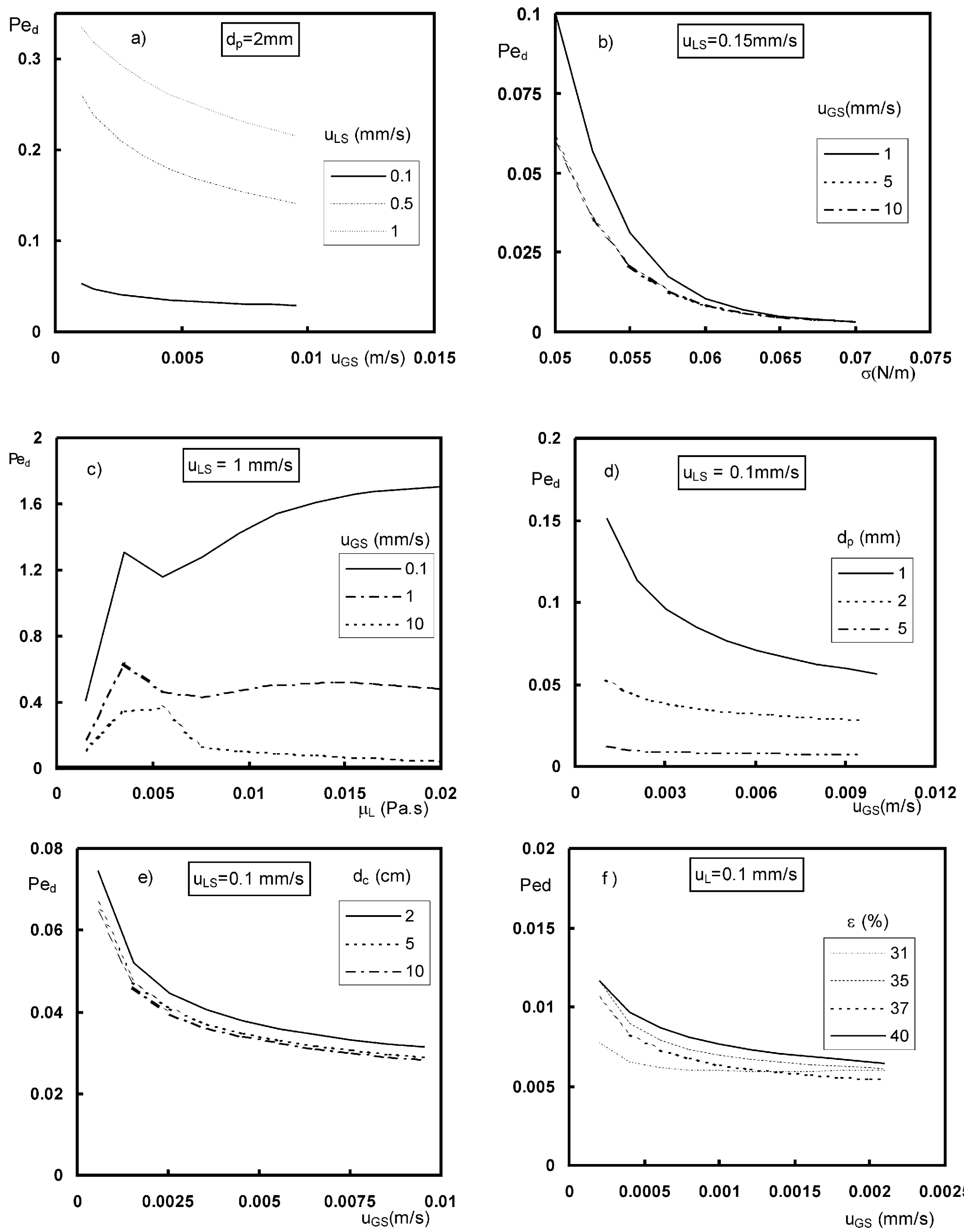

Fig. 3. Simulations of fluid and bed properties on Pe_d. Effect of: (a) gas and liquid velocities, (b) surface tension, (c) liquid viscosity, (d) particle diameter, (e) column diameter, (f) bed porosity.

Table 8
Entry keys for Péclet number simulations shown in Fig. 3

Fig. 3	u_{GS} (mm/s)	u_{LS} (mm/s)	ρ_G (kg/m^3)	μ_G (Pa s × 10^5)	ρ_L (kg/m^3)	μ_L (Pa s × 10^3)	σ_L (N/m × 10^3)	d_p (m × 10^3)	d_C (m × 10^2)	ε (%)
a	**0→15**	**0.1; 0.5; 1**	1.2	1.82	1000	1	72	2	5	35
b	1; 5; 10	0.15	1.2	1.82	1000	1	**50→72**	3.5	5	35
c	0.1; 1; 10	1	1.2	1.82	1000	**1→20**	72	5	5	35
d	0 → 12	0.1	1.2	1.82	1000	1	72	**1; 2; 5**	5	40
e	0 → 10	0.1	1.2	1.82	1000	1	72	2	**1; 5;10**	40
f	0 → 2.5	0.1	1.2	1.82	1000	1	72	2	5	**31→40**

neural network correlation. This is supported by the experimental results of van Gelder and Westerterp [19] and of Thanos et al. [6] which confirm that the liquid mixing is affected neither by the pressure level (up to 5.3 MPa) nor by the type of gas phase (H_2 vs. N_2).

The effect of liquid and gas superficial velocity is illustrated in Fig. 3a. As expected, liquid back-mixing is promoted by decreasing liquid velocities. Also, Pe_d decreases as u_{GS} increases until a critical gas velocity, corresponding to the onset of pulsing, above which u_{GS} effect becomes marginal. As reported by Iliuta et al. [28], the superficial gas velocity affects the Péclet number especially in the bubble flow regime due to the macro-circulation flow patterns induced by the bubbles. These simulations are supported by experimental observations from [6,28].

The surface tension effect is shown in Fig. 3b which suggests that a low surface tension liquid induces a higher Péclet number than a high surface tension liquid. This is in agreement with Weber [13] experimental observations. A simplistic but realistic interpretation could be that bubbles cannot oppose to the surrounding liquid shear field; as a result of a low liquid surface tension, they erode easily into small bubbles. More uniform small bubbles rising slowly up the bed produce less back-mixing in the liquid.

Contrary to the surface tension, the effect of liquid viscosity is not monotonous as shown in Fig. 3c. The studies summarized in the databank reveal indeed conflicting trends. Bezdenezhnykh et al. [15] observed a decrease of Pe_d when the liquid viscosity is increased from water to glycerin. Cassanello et al. [22] observed an increase of Pe_d with sucrose solutions of increasing viscosity. Iliuta et al. [25] reported that for non-porous particles, Pe_d increases with an increase of the aqueous CMC consistency index, whereas for the same conditions, Pe_d decreases in the case of porous particles.

In accordance with Weber [13] observations larger particles lead to lower Péclet numbers (Fig. 3d), whereas the column diameter (Fig. 3e) and the bed porosity (Fig. 3f) effects are negligible in accordance with [15,20,26].

5. Conclusion

Based on a liquid axial dispersion coefficients databank, a Péclet number correlation was developed using artificial neural network modeling and dimensional analysis. The prediction of *Pe* was significantly improved. The effect on axial dispersion of dominant operating variables such as gas and liquid velocities, surface tension and particle size was clearly identified while other characteristics such as liquid viscosity and bed porosity require specific studies.

Acknowledgements

Financial support from the Natural Sciences and Engineering Research Council of Canada (NSERC) and the Fonds pour la Formation de Chercheurs et d'Aide à la Recherche (Québec) is gratefully acknowledged.

References

[1] A. Germain, G.A. L'Homme, A. Lefebvre, in: G.A. L'Homme (Ed.), Chemical Engineering of Gas–Liquid–Solid Catalyst Reactions, CEBEDOC, Liège, Belgium, 1979, p. 265.
[2] P. Trambouze, Rev. Inst. Franç. Petr. 46 (1991) 433.
[3] K.B. van Gelder, J.K. Damhof, K.R. Westerterp, Chem. Eng. Sci. 45 (1990) 3171.
[4] F. Stüber, A.M. Wilhelm, H. Delmas, Chem. Eng. Sci. 51 (1996) 2161.

[5] S.T. Sie, Rev. Inst. Franç. Petr. 46 (1991) 501.
[6] A.M. Thanos, P. Menagias, P.A. Galtier, N.G. Papayannakos, Ind. Eng. Chem. Res. 38 (1999) 3817.
[7] Z. Bensetiti, F. Larachi, B.P.A. Grandjean, G. Wild, Chem. Eng. Sci. 52 (1997) 4239.
[8] F. Larachi, Z. Bensetiti, B.P.A. Grandjean, G. Wild, Chem. Eng. Technol. 21 (1998) 887.
[9] A. Gianetto, G. Baldi, V. Specchia, S. Sicardi, AIChE J. 24 (1978) 1087.
[10] Y.T. Shah, Gas–Liquid–Solid Reactor Design, McGraw-Hill, New York, 1979.
[11] T.B. Zhukova, V.N. Pisarenko, V.V. Kafarov, Int. Chem. Eng. 30 (1990) 57.
[12] W. Bill, Diplomarbeit, Technischen Hochschule, Darmstadt, Germany, 1955.
[13] H.H. Weber, Untersuchungen über die Verweilzeitverteilung in Aufstromkolonnen, Ph.D. Dissertation, Technischen Hochschule, Darmstadt, Germany, 1961.
[14] W. von Heilmann, H. Hofmann, Proceedings of the Fourth European Symposium Chemical Reactor Engineering, Brussels, Belgium, 1969, p. 169.
[15] A.A. Bezdenezhnykh, V.I. Taranov, A.P. Orlov, Teor. Osn. Khim. Tekhnol. 5 (1971) 163.
[16] G.J. Stiegel, Y.T. Shah, Ind. Eng. Chem. Process. Des. Dev. 16 (1977) 37.
[17] G.J. Stiegel, Y.T. Shah, Can. J. Chem. Eng. 55 (1977) 3.
[18] S.K. Achwal, J.B. Stepanek, Can. J. Chem. Eng. 57 (1979) 409.
[19] K.B. van Gelder, K.R. Westerterp, Chem. Eng. Technol. 13 (1990) 27.
[20] A.M. Thanos, P.A. Galtier, N.G. Papayannakos, Chem. Eng. Sci. 51 (1996) 2709.
[21] M.C. Cassanello, Caracterización fluidodinámica de reactores trifásicos de lecho fijo, Ph.D. Thesis, Universidad de Buenos Aires, Buenos Aires, Argentina, 1992.
[22] M. Cassanello, O. Martinez, A.L. Cukierman, Chem. Eng. Sci. 53 (1998) 1015.
[23] Y.T. Shah, G.J. Stiegel, M.M. Sharma, AIChE J. 24 (1978) 369.
[24] V.B. Skomorokov, V.A. Kirillov, G. Baldi, Chem. Eng. J. 33 (1986) 169.
[25] I. Illiuta, F.C. Thyrion, O. Muntean, M. Gigot, Chem. Eng. Sci. 51 (1996) 4579.
[26] X.-L. Yang, J.P. Euzen, G. Wild, Chem. Eng. Sci. 45 (1990) 3311.
[27] X.-L. Yang, Études hydrodynamiques des réacteurs à lit fixe avec écoulement co-courant ascendant de gaz et de liquide, Ph.D. Thesis, Université Pierre et Marie Curie (Paris IV) and ENSPM, France, 1989.
[28] I. Illiuta, F.C. Thyrion, O. Muntean, Trans. Inst. Chem. Eng. 76 (1998) 64.
[29] I. Illiuta, F.C. Thyrion, L. Bolle, M. Giot, Chem. Eng. Technol. 20 (1997) 171.
[30] I. Iliuta, F. Larachi, B.P.A. Grandjean, Chem. Eng. Sci. 54 (1999) 4099.
[31] K. Haga, Y. Niibori, T. Childa, Water Resour. Res. 35 (1999) 1065.
[32] A.M. Thanos, P.A. Galtier, N.G. Papayannakos, Chem. Eng. Sci. 54 (1999) 2781.
[33] V.A. Kirillov, M.A. Kasamanyan, V.A. Kuzin, Theoret. Fundam. Chem. Eng. 9 (1975) 870.
[34] F. Stüber, Sélectivité en réacteur catalytique triphasique: analyse expérimentale et théorique d'hydrogénations consécutives en lit fixe catalytique à co-courant ascendant de gaz et de liquide, Ph.D. Thesis, Institut National Polytechnique de Toulouse, France, 1995.
[35] Syaiful, Réacteurs polyphasiqueà co-courant ascendant : influence de la viscosité sur les rétentions, dispersions axiales, et transfert gaz-liquide', Ph.D. Thesis, Institut National Polytechnique de Toulouse, France, 1993.